NASA TECHNICAL NOTE

NASA TN D-4417

C.1

NASA TN D-4417

DYNAMIC PRESSURE LIMITS FOR FLAT PLATES AS RELATED TO NUCLEAR FUEL ELEMENTS

by Roger L. Smith

Lewis Research Center

Cleveland, Ohio

NATIONAL AERONAUTICS AND SPACE ADMINISTRATION • WASHINGTON, D. C. • FEBRUARY 1968

DYNAMIC PRESSURE LIMITS FOR FLAT PLATES AS RELATED TO NUCLEAR FUEL ELEMENTS

By Roger L. Smith

Lewis Research Center
Cleveland, Ohio

NATIONAL AERONAUTICS AND SPACE ADMINISTRATION

For sale by the Clearinghouse for Federal Scientific and Technical Information
Springfield, Virginia 22151 – CFSTI price $3.00

DYNAMIC PRESSURE LIMITS FOR FLAT PLATES AS RELATED TO NUCLEAR FUEL ELEMENTS

by Roger L. Smith

Lewis Research Center

SUMMARY

Tests with air or helium flowing over single flat plates were performed at room temperature to determine the values of dynamic pressure required to cause plate failure. Failure was defined as a deflection greater than 0.010 inch (0.254 mm).

The ranges of the dimensions used were as follows: plate thickness, 0.020 to 0.040 inch (0.508 to 1.02 mm); plate length, 0.5 to 4.0 inches (1.27 to 10.2 cm); plate width, 1.2 to 2.0 inches (3.05 to 5.08 cm); and flow-channel height, 0.038 to 0.091 inch (0.96 to 2.31 mm). The plate materials selected were lead, aluminum, copper, and steel, which provide ranges of Young's modulus of elasticity from 2×10^6 to 30×10^6 psi (1.38×10^6 to 20.7×10^6 N/cm^2), and of Poisson's ratio from 0.288 to 0.42. Gas density varied from 0.025 to 1.0 pound per cubic foot (0.4 to 16 kg/m^3).

The experimental results were compared with an existing theoretical analysis which predicts dynamic pressure for sudden, complete plate collapse. The experimental results agree with the theoretical prediction for the effect of the material properties, but disagree with the prediction for the effect of the plate and flow-channel dimensions. The large amount of experimental data scatter and the disagreement of these data with the theoretical prediction may be caused by leading-edge effect, flutter, turbulence, or other unknown factors.

INTRODUCTION

Various investigators have studied the problem of collapse of parallel-plate fuel elements at high coolant velocities in nuclear reactors. Some early experiments on this problem are described in references 1 and 2. One explanation for plate collapse was proposed by D. R. Miller in reference 3. This analysis postulates that at some critical fluid velocity the pressure forces on either side of the plate become unbalanced to the extent that collapse occurs.

In further analytical work, E. B. Johansson (ref. 4) considered the effects of flow redistribution and unequal friction pressure drop in the flow channels. Also, J. J. Kane (ref. 5) has done some analytical work on the effect of inlet spacing deviations. To confirm Miller's analysis, W. L. Zabriskie (refs. 6 and 7) conducted experiments with water flowing over aluminum and clear plastic plates. These limited experimental results agreed reasonably well with the prediction of critical velocities from Miller's analysis.

This investigation comprises a further and more extensive series of tests. Several plate materials and plate dimensions were used. For each combination of material and dimensions, several plates were fabricated, and each was individually subjected to increasing gas flow at room temperature until it failed. Plate failure was defined as either a center upstream-edge deflection of 0.010 inch (0.254 mm) or complete plate collapse. The velocity at failure in terms of dynamic pressure was correlated as a function of material property and of plate geometry parameters suggested by Miller (ref. 3).

The scope of the experiments included plate thicknesses from 0.020 to 0.040 inch (0.508 to 1.02 mm); plate lengths from 0.5 to 4.0 inches (1.27 to 10.2 cm); plate widths from 1.2 to 2.0 inches (3.05 to 5.08 cm); flow-channel heights from 0.038 to 0.091 inch (0.96 to 2.31 mm); and gas (helium or air) densities from 0.025 to 1.0 pound per cubic foot (0.4 to 16 kg/m^3). The plate materials selected were lead, aluminum, copper, and steel, which provided ranges of Young's modulus of elasticity from 2×10^6 to 30×10^6 psi (1.38×10^6 to 20.7×10^6 N/cm^2) and of Poisson's ratio from 0.288 to 0.42.

Edge-effect calculations are discussed in an appendix by A. F. Lietzke.

SYMBOLS

A	total cross-sectional flow area at the plate
a	plate thickness
b	plate span
E	Young's modulus of elasticity
g	gravitational constant
h	flow-channel height
l	effective plate length, $\leq b$
p	pressure
q	dynamic pressure, $\rho V^2/2g$
q_c	critical dynamic pressure, $\rho V_c^2/2g$
V	velocity

V_c critical velocity

w weight flow rate

ρ weight density of gas at plate

ν Poisson's ratio

ANALYTICAL CONSIDERATIONS

This section describes the basic features and assumptions of Miller's analysis (ref. 3) which led to his equation for predicting critical velocity for failure of multiple parallel plates and single flat plates. A modification to Miller's equation for critical velocity is proposed. This equation is expressed in terms of critical dynamic pressure, the parameter of interest herein.

Miller Analysis

This analysis "applies the Bernoulli theorem for incompressible flow to determine the pressure differences which would be developed across the plates by modification of local fluid velocities as a result of plate deflections. Equating these pressure differences to those which would be required to produce the corresponding deflections (as in a beam) gives an expression for the critical velocity in terms of plate and fluid parameters" (ref. 3). The initial deflections could be caused by gas flow turbulence or imperfections in the hardware; there is always some perturbation present to initiate a plate deflection.

The assumptions were as follows:

"1. The plates are homogeneous, isotropic, elastic, initially flat . . . , uniform in spacing and dimensions, and free of unidentified sources of deformation.

2. The coolant is incompressible; all channels have the same mass flow; at any cross section normal to the longitudinal axis the flow within any channel is uniform; and leakage between channels is suppressed.

3. Plates are broad enough in comparison with their thickness that shear deformation is negligible, and are long enough in comparison with their breadth that plates can deflect locally without significant redistribution of flow among the coolant channels.

4. Side plates or supports are rigid."

The final equation for the case of multiple parallel flat plates with built-in edges is

$$V_c = \left[\frac{15g\,Ea^3h}{\rho b^4(1 - \nu^2)}\right]^{1/2} \tag{1}$$

The analysis indicates that V_c^2 (and therefore critical dynamic pressure q_c) for single flat plates is twice that given by equation (1) for multiple parallel flat plates. The equation for a single plate can be written in terms of critical dynamic pressure as follows:

$$q_c = \frac{15E}{1 - \nu^2}\,\frac{a^3h}{b^4} \tag{2}$$

The first term on the right side is the plate material parameter (function of material properties); the second term is the plate geometry parameter (function of plate and passage dimensions).

Limitations of Miller Analysis

Nonideal conditions. - It seems obvious that the assumed ideal conditions cannot exist in an actual experiment. The variations from ideal conditions, especially regarding uniformity of dimensions, materials, and flow, would be expected to cause experimental plate failure to occur at a lower dynamic pressure than the ideal value predicted by the analysis. Since an incompressible fluid was assumed in the analysis, the Mach number for the tests reported herein was kept below 0.4 to minimize compressibility effects.

By assuming the plate to be a wide beam, the analysis neglects any local effects occurring in the vicinity of the upstream or downstream edges of the plate. In fact, reference 3 states that "If the plates are deflected over a longitudinal distance several times the width of the plates, then near the center of the deflected portion of a plate the longitudinal variations in deflection can be neglected, ..." The analysis then goes on to consider the central portion of the plate.

At the upstream and downstream edges, the plate is no longer, in effect, a wide beam, and the deflection at these edges will be greater than that calculated in the analysis. The calculations for this greater deflection and its effect on dynamic pressure are shown in the appendix. In order to incorporate these effects it is necessary to modify equation (2) as given by the following equation from the appendix:

$$q_c = \left(\frac{15E}{1 - \nu^2}\right)\left(\frac{a^3 h}{b^4}\right)\left[\frac{1}{\left(1 + \frac{4\pi\nu l h}{b^2}\right)\left(1 + \frac{4\nu l^2}{3b^2}\right)}\right] \tag{12}$$

Failure criterion. - Since these experiments were intended to measure the dynamic pressure required to produce plate failure, some criterion of plate failure was needed. Although the analysis indicates that once failure is initiated a sudden and complete collapse of the plate would occur, this did not happen in many of the cases reported here and elsewhere (ref. 6). Often the deflection of the upstream edge of the plate would gradually increase with an increase in flow. Little deflection occurred in the downstream edge.

A somewhat arbitrary center-upstream-edge deflection of 0.010 inch (0.254 mm) was used as the failure criterion for gradual failures to obtain meaningful data for nuclear reactor fuel-element design. For this deflection some of the outer fibers of the aluminum, copper, and lead plates will have stretched past their yield point, while no yield will have occurred in the steel plates. For the extreme cases less than half the plate remains in the elastic condition when deflected 0.010 inch (0.254 mm) at the center.

Electrical contacts described in Electrical instrumentation section and placed at the upstream edge of the plate signaled when the center-upstream-edge deflection had reached 0.010 inch (0.254 mm). As mentioned in the INTRODUCTION, earlier tests (e.g., ref. 6) showed that failure nearly always occurred first at this location.

In the investigation of the effect of upstream-edge support, the plate always failed suddenly in a gross manner. This failure was easily observed with the instrumentation, so no arbitrary definition of failure was required.

APPARATUS

The apparatus used for these tests consisted of the piping system, the plate holder, and the instrumentation.

Piping System

The piping system is shown in figure 1. The inlet end of the system was connected to the laboratory gas supply with 4-inch (10.2-cm) pipe. The outlet end was connected to atmosphere outside the building with 6-inch (15.2-cm) pipe. Within this piping sys-

tem, the gas flowed through the orifice section, the inlet control valve, the test section which contained the plate-holder assembly and test plate, and the outlet control valve.

Immediately downstream of the inlet connection was a standard ASME orifice section for measuring the gas flow rate. Pneumatically operated valves, to control both pressure level and flow rate, were placed both upstream and downstream of the test plate (fig. 1). These 2-inch (5.08-cm) plug-type valves were remotely operated from the control panel.

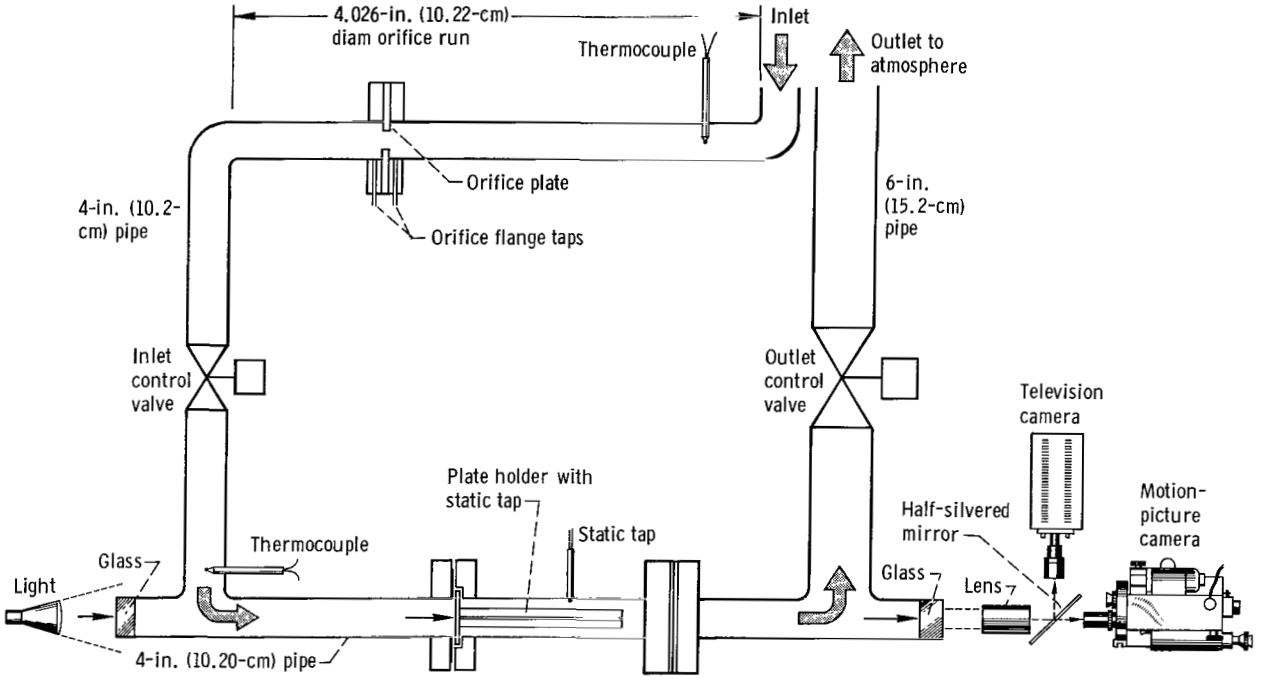

Figure 1. - Schematic diagram of test apparatus for single-plate flow tests.

The plate-holder mounting section was stationed between two pipe tees (fig. 1), each of which contained a sight glass to permit plate illumination and observation. This mounting section was a spool piece about 1 foot (30.5 cm) long, with the plate-holder assembly mounted to it. For most of the tests, this spool piece was made of steel. However, for the tests utilizing high-speed moving pictures of the plate, this spool piece was made of clear plastic.

Plate-Holder Assembly

Figure 2 shows the plate-holder assembly. This holder was made of stainless steel machined to a thickness of 0.30 inch (7.62 mm) with bolt holes spaced 1.75 inches (4.44 cm) apart except at the plate location. The plate holder extended 7.75 inches (19.7 cm) upstream of the plate for a ratio of length to hydraulic diameter greater than 20. This extension allowed ample length to develop undisturbed flow at the upstream edge of the plate being tested. The flow-passage surfaces were painted flat black to reduce reflections.

Two important features of the holder are shown in figure 2(a). One is the contact point located 0.0625 inch (1.59 mm) downstream from the leading edge of the plate, which was used to indicate electrically a plate failure. This contact was also used to point support the upstream edge when desired. The other feature is the wall static pressure tap, a 0.0312-inch- (0.794-mm-) diameter hole, perpendicular to the surface and 0.5 inch (1.27 cm) upstream of the leading edge of the plate.

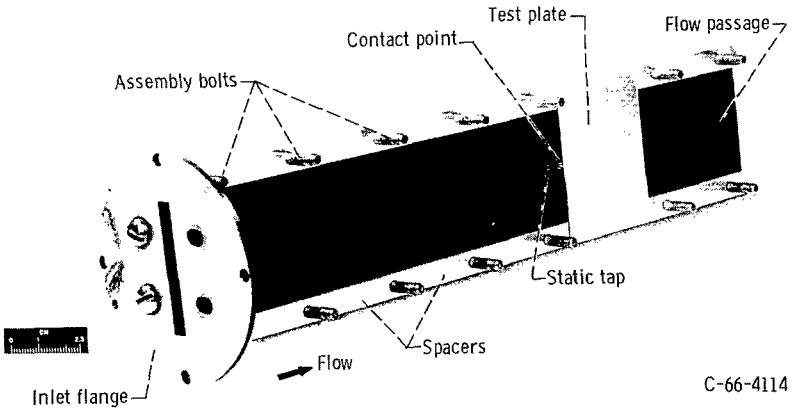

(a) View of diassembled holder with test plate in position.

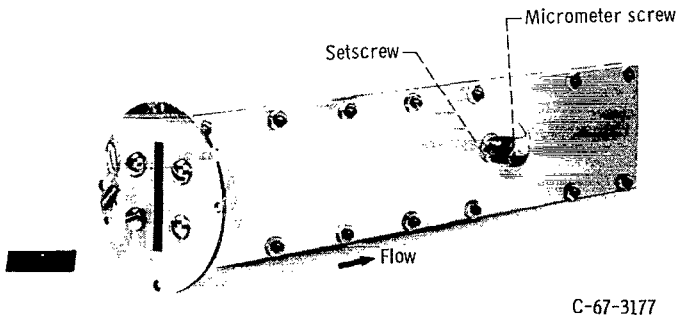

(b) Outside view of assembly with micrometer for contact adjustment.

Figure 2. - Plate holder for single-plate tests.

Figure 2(b) shows the outside of the assembly with the micrometer for electrical contact adjustment. The other side had a similar adjustable electrical contact, and each micrometer head had a setscrew to hold it in position.

Figure 3 is an enlarged schematic diagram of the plate holder with a typical spacer arrangement. The 0.003-inch (0.076-mm) clearance was used so that the plate being tested would not be firmly held. Miller's analysis does not allow for the tension forces which fixed ends would cause. Variation of the width as well as the thickness of the other spacers above and below the test plate produced the desired variations in plate span and flow-channel height. Spacers of clear plastic were used when the high-speed moving pictures were taken.

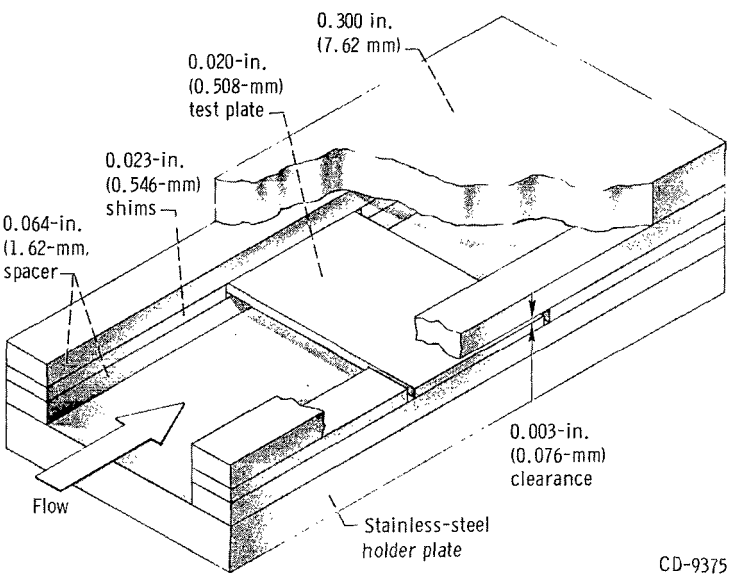

Figure 3. - Typical spacer arrangement.

Instrumentation

Four types of instrumentation provided the data required from these tests: pressure, temperature, optical, and electrical.

Pressure instrumentation. - Static pressure taps were placed at four locations (fig. 1): two in the orifice flanges, one in the plate-holder assembly, and one in the spool piece surrounding the plate holder. These taps were connected by copper tubing to indicating devices. Calibrated pressure gages indicated upstream orifice pressure and upstream test-plate pressure. Mercury manometers indicated pressure drop across the orifice plate and test plate. The pressure gage and manometer indications were recorded

manually. The two pressure differentials and the upstream test-plate pressure were also measured with pressure transducers and recorded on strip-chart recorders.

Temperature instrumentation. - Iron-constantan thermocouples were used at two locations (fig. 1) to measure orifice air temperature and test-section inlet temperature. These temperatures were indicated on a null-type potentiometer and recorded manually.

Optical instrumentation. - The optical system (fig. 1) provided visual monitoring of the plate during testing. Light shining through special high-strength glass illuminated the test plate. Another glass transmitted the image of plate and contact points to the camera by means of the lens and half-silvered mirror. This mirror transmitted part of the light to a movie camera and reflected the other part to a television camera. The test operator monitored the image on a panel-mounted television screen.

For the high-speed moving pictures of the side edge of the test plate, the camera was placed to view perpendicular to the flow through the clear plastic spacers and spool piece. Illumination came from behind so that a silhouette of the plate edge was observed.

Electrical instrumentation. - Micrometer-adjusted electrical contacts were provided in the plate-holder assembly to indicate plate failure. These contacts were connected to one of the following indicating devices: an ohmmeter, an oscilloscope, or a buzzer. The ohmmeter was used for most of the tests.

PROCEDURE

This section describes the procedures used to prepare the plates for testing, to test the plates to failure, and to reduce the experimental data to values of dynamic pressure.

Plate Preparation

The processing of the plates to be tested was carefully controlled to ensure maximum uniformity. The lead, aluminum, and copper plates were rolled to within 0.001 inch (0.0254 mm) of the specified thickness and sheared to size. The aluminum and copper plates were then annealed in a furnace while clamped between flat steel plates to make them as flat and as uniform in their properties as possible. Each lead plate was flattened by placing it on a flat surface and rubbing it. Since annealing takes place in lead at room temperature, the lead plate became annealed shortly after flattening. Each steel plate was cut from the same piece of flat-sheet spring stock which was the right thickness when received; the steel plates were not annealed. Finally, the upstream edge of each plate was always deburred but left square. Micrometer calipers were used to measure the thickness of each plate.

Testing

The test plate was installed in the plate-holder assembly and the bolts were always tightened to a torque of 25 inch-pounds (282 N-cm). The contact points were each successively advanced until electrical contact with the plate was made. Each point was then retracted 0.010 inch (0.254 mm) with the micrometers and was clamped in position with setscrews. The holder assembly was then inserted into the test-section spool piece (fig. 1).

The test was started by opening the inlet control valve and setting the desired pressure level with a small gas flow rate. At this condition a data point was taken for reference, and the movie camera was turned on. While constant pressure was maintained, gas flow rate was slowly increased until either (1) contact was indicated between the test plate and the micrometer-adjusted contact or (2) the plate failed suddenly as indicated visually or by system pressure changes. One of these conditions represented plate failure, and data were again recorded. The elapsed time from first data point to failure point was usually about 2 minutes.

Data Reduction

The gas flow rate w was measured by using a standard ASME orifice run. Accordingly, orifice calibration curves provided the gas flow rate as a function of orifice flow coefficients, orifice size, orifice upstream gas density, and measured pressure drop across the orifice plate. The temperature-measuring thermocouples were located in large-area, low-velocity sections of the pipe; therefore, the temperature measured is static temperature.

With the flow rate known, the velocity was calculated from the continuity equation

$$V = \frac{w}{\rho A} \tag{3}$$

and the dynamic pressure was calculated from the equation

$$q = \frac{\rho V^2}{2g} \tag{4}$$

The gas density and flow area were evaluated at the test plate.

RESULTS AND DISCUSSION

The geometry and material effects are presented herein, followed by a comparison of the experimental data with the theoretical prediction. Then other effects - plate length, gas density, initial plate distortion, and upstream-edge support - are presented. Finally, the different modes of plate failure are discussed.

The data for dynamic pressure at failure are plotted as functions of the variables and parameters of equations (2) and (12). The parameter $E/(1 - \nu^2)$ is called the plate material parameter and is a property of the plate material. The parameter a^3h/b^4 is called the plate geometry parameter since it is a function of the geometry factors. The averages presented are arithmetical averages.

Geometry Effects

The dimensions which were varied to study geometry effects were plate thickness, plate span, and flow-channel height. Aluminum was chosen as the plate material to study these variables. The material parameter $E/(1 - \nu^2)$ for aluminum has a constant value of 1.12×10^7 psi (7.73×10^6 N/cm^2). For these tests, plate length was 2.0 inches (5.08 cm) and gas density was about 1.0 pound per cubic foot (16 kg/m^3).

Plate thickness. - The effect of plate thickness on dynamic pressure at failure is shown in figure 4(a). Plate width and flow-channel height were held constant, while plate thickness was varied from 0.020 to 0.040 inch (0.508 to 1.02 mm). The individual data points as well as average values for each thickness group are shown. The data show considerable scatter. The dynamic pressure at failure increased approximately as the second power of the thickness as indicated by the solid line drawn near the mean values.

Plate span. - The effect of plate span, or width, on dynamic pressure at failure is shown in figure 4(b). The plate span was varied from 1.2 to 2.0 inches (3.05 to 5.08 cm) with plate thickness and flow-channel height held constant. Again, the experimental data show considerable scatter. Dynamic pressure at failure increased approximately as $1/(b^{2.8})$, where b is plate span.

Flow-channel height. - The effect of flow-channel height on dynamic pressure at failure is shown in figure 4(c). The heights used were 0.038, 0.064, and 0.091 inch (0.96, 1.62, and 2.31 mm, respectively), with plate thickness and span held constant. Here also, there is considerable scatter in the data. The dynamic pressure at failure increased approximately with flow-channel height to the 0.61 power.

Geometry parameter. - The thickness, span, and flow-channel height data, along with applicable data points from references 6 and 7, are presented in figure 5. Here the ratio of dynamic pressure at failure to plate material parameter is plotted against the plate

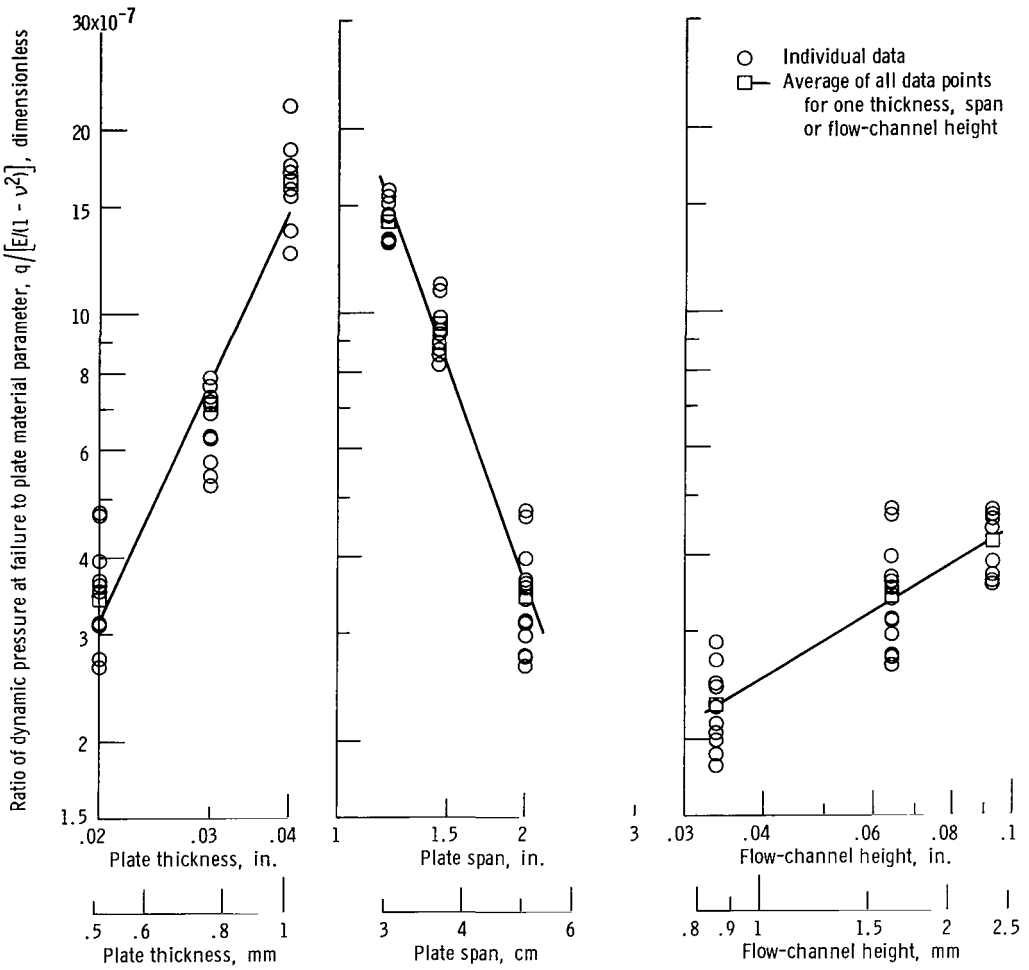

(a) Plate thickness. Flow-channel height, 0.064 inch (1.62 mm); plate span, 2.0 inches (5.08 cm).

(b) Plate span. Plate thickness, 0.020 inch (0.508 mm); flow-channel height, 0.64 inch (1.62 mm).

(c) Flow channel height. Plate span, 2.0 inches (5.08 cm); plate thickness, 0.020 inch (0.508 mm).

Figure 4. - Effect of geometry factors on dynamic pressure at failure. Plate material, aluminum; approximate gas density, 1.0 pound per cubic foot (16 kg/m^3).

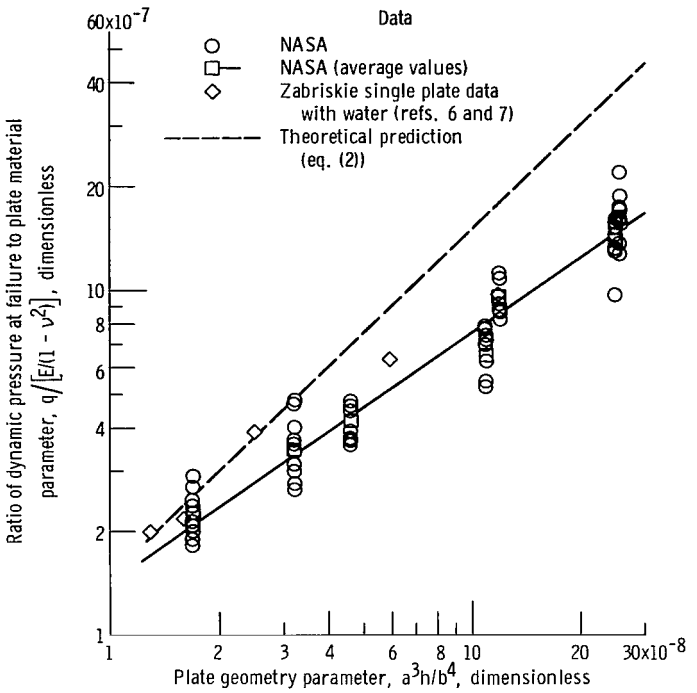

Figure 5. - Combination of aluminum data for geometry parameter effect. Approximate gas density, 1.0 pound per cubic foot (16 kg/m^3).

geometry parameter (see eq. (2)). A solid line is drawn near the average points and has a slope of about 0.72 as compared with the theoretical slope of 1.0.

Material Effects

The experimental data for four materials, lead, aluminum, copper, and steel, are shown in figure 6. Dynamic pressure at failure is plotted against the plate material parameter while the geometry parameter is held constant at 3.21×10^{-8}. The solid line drawn through the data points shows that the dynamic pressure at failure increases almost in direct proportion to the material parameter, as predicted by equation (2).

Comparison of Experimental Data with Theoretical Prediction

Figure 7(a) is a combined plot of all the data presented previously for both material and geometry effects. The square data points represent the arithmetical mean values for

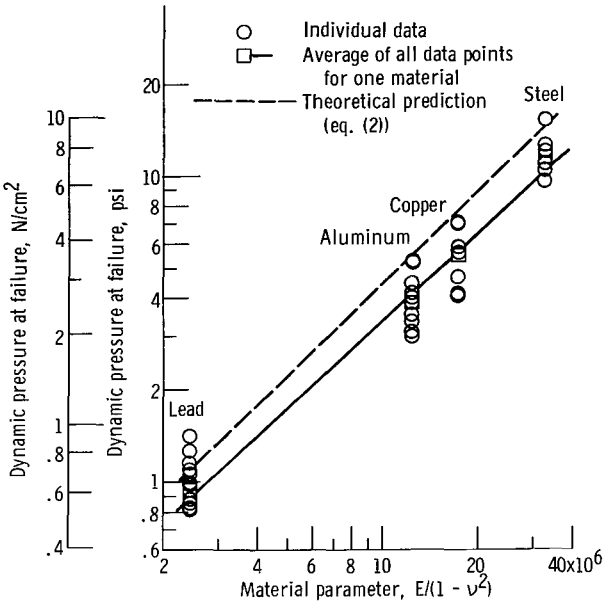

Figure 6. - Combination of data for materials parameter effect. Plate geometry parameter, 3.21×10^{-8}; approximate gas density, 1.0 pound per cubic foot (16 kg/m^3).

the various materials, while the vertical lines through these points indicate the range of data scatter. Also shown is the line of Miller's theoretical prediction (eq. (2)) and the water-flow data points from references 6 and 7, indicated by the circular symbols. The solid line drawn through the experimental averages has a slope of about 0.68 compared with a slope of 1.0 for the theoretical line.

The geometry parameter effect is the principal cause of the difference between the experimental and theoretically predicted results. A comparison of figures 5 and 6 shows that the theoretical analysis predicts the material parameter effect quite well but poorly predicts the geometry parameter effect. Figure 7(b) shows the same data as figure 7(a) but uses the edge-effect modification applied to the plate geometry parameter. This modification is partly a function of plate length l and Poisson's ratio ν, neither of which were originally included in the geometry parameter. The effect of the correction factor resulting from consideration of these edge (and also, therefore, length) effects can be seen by comparing the two parts of figure 7. The slope of the experimental line in figure 7(b) is about 0.78 compared with 0.68 for the line (fig. 7(a)) which was not corrected for edge effect. Thus, the correction factor helps to give a better theoretical prediction. Since this prediction still differs from the experimental results, there must remain some unknown factors affecting plate failure. Some of these factors may be other leading-edge effects, flutter, and turbulence. These same factors also could contribute to the data scatter.

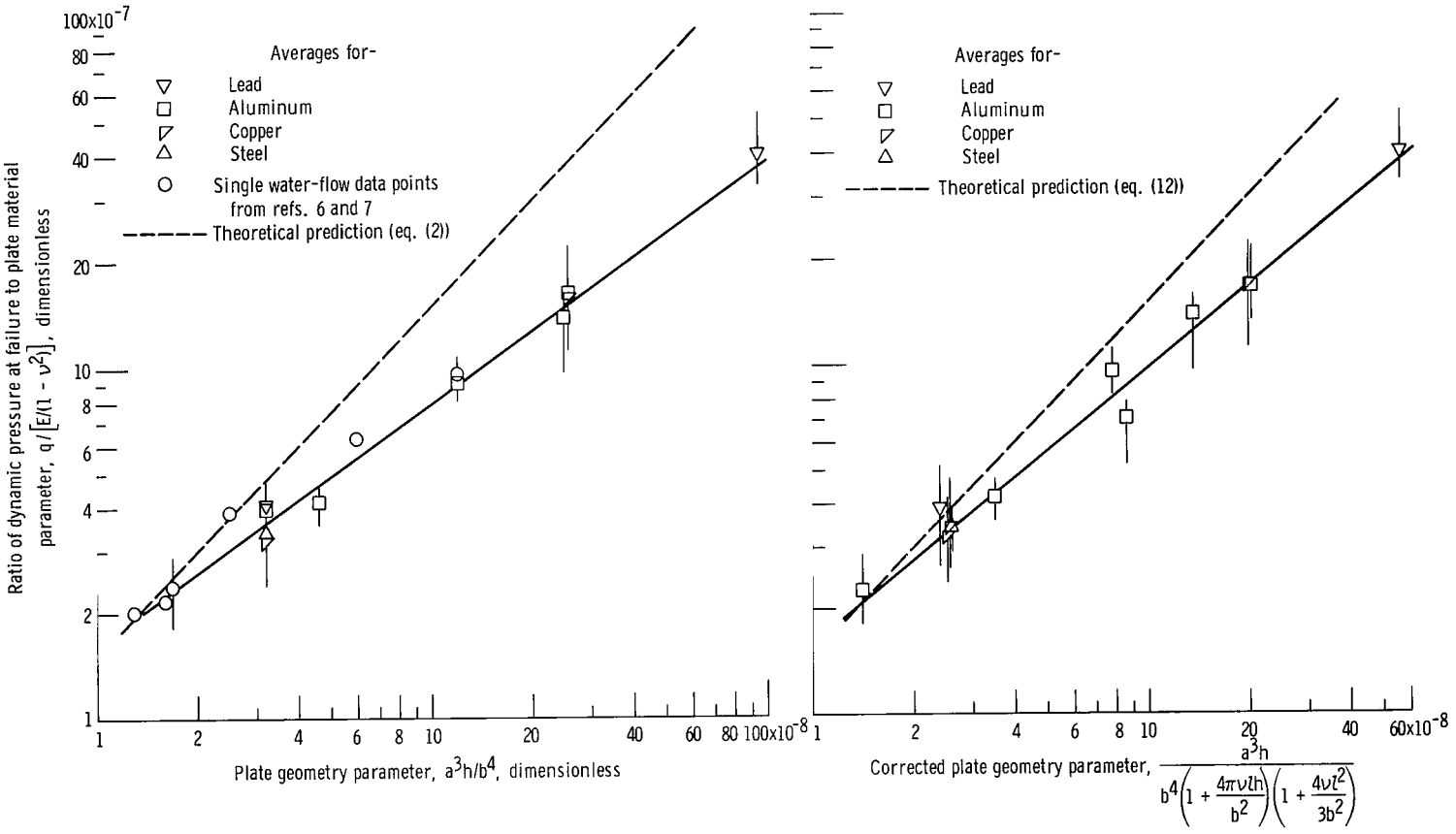

(a) Data not corrected for edge effect.

(b) Data corrected for edge effect.

Figure 7. - Comparison of theoretical prediction with combined data for all materials and geometries tested. Approximate gas density, 1.0 pound per cubic foot (16 kg/m^3).

Other Effects

Plate length. - The effect of plate length on dynamic pressure at failure was determined by testing plates 0.5, 2, and 4 inches (1.27, 5.08, and 10.2 cm, respectively) long. Also, a 48-inch (122-cm) length was simulated by placing a flow restrictor at the downstream end of a 4-inch- (10.2-cm-) long plate; the restrictor pressure drop was equivalent to that for a 48-inch (122-cm) passage length. Figure 8 shows that measured dynamic

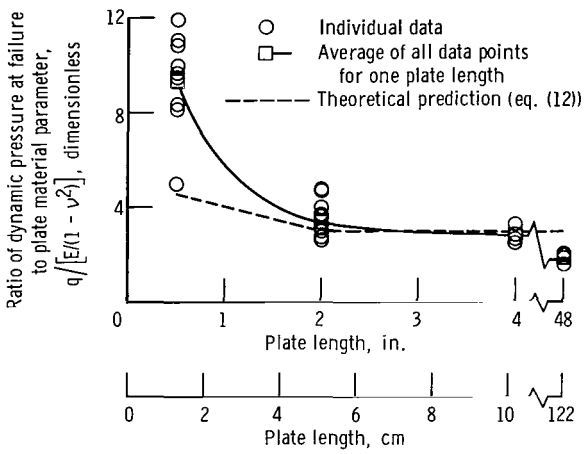

Figure 8. - Effect of plate length in flow direction on dynamic pressure at failure. Plate material, aluminum; plate thickness, 0.020 inch (0.508 mm); plate span, 2.0 inches (5.08 cm); flow-channel height, 0.064 inch (1.62 mm); approximate gas density, 1.0 pound per cubic foot (16 kg/m^3). The 48-inch (122-cm) length was calculated.

pressure at failure (divided by a constant material parameter of 1.12×10^7 psi (7.73×10^6 N/cm^2)) decreases as plate length increases. These data follow quite closely the theoretical prediction (see appendix) except for short lengths. Flow redistribution may account for the divergence of the data at short lengths, since the theory assumes no flow redistribution.

Gas density. - The density of the hydrogen coolant in a nuclear rocket reactor would be orders of magnitude less than the convenient density for room-temperature tests of about 1.0 pound per cubic foot (16 kg/m^3). Therefore, density-effect tests were undertaken. The effect of gas density on dynamic pressure at failure was evaluated using helium and air at several pressure levels. The result is shown in figure 9. The influence of gas density appears relatively minor compared with other unknown factors that cause great data scatter.

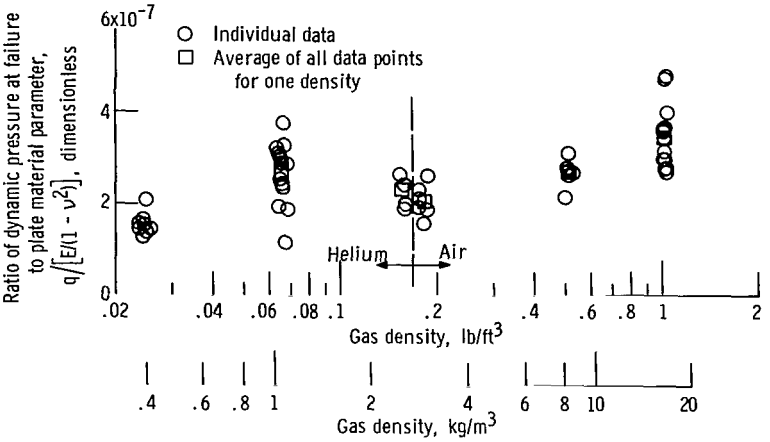

Figure 9. - Effect of gas density on dynamic pressure at failure. Plate material, aluminum; plate thickness, 0.020 inch (0.508 mm); plate span and length in flow direction, 2.0 inches (5.08 cm); flow-channel height, 0.094 inch (1.62 mm).

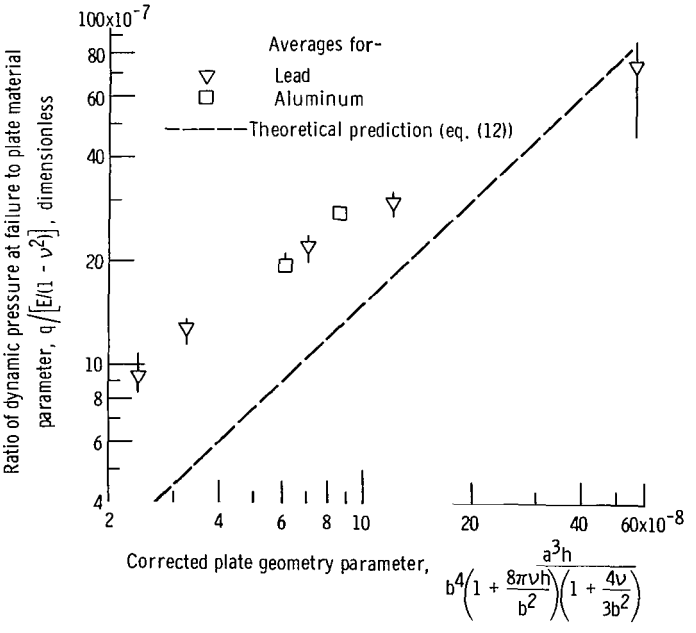

Figure 10. - Effect of supported upstream edge. Plate length, 4.0 inches (10.2 cm); approximate gas density, 1.0 pound per cubic foot (16 kg/m^3).

Initial plate distortion. - The initial micrometer settings of the contact points were tabulated for the data from five different geometry parameters. From this data the off-center position of the plate was calculated. In each group the most off-center plate did not give a data point at the extremities of the scatter. Thus, initial lack of flatness is apparently not an important factor in the scatter of the data points.

Upstream-edge support. - In an attempt to eliminate leading-edge effect, seven series of tests were made with the upstream edge supported at the center by the electrical contacts. These contacts were about 0.03 inch (0.762 mm) in diameter, and the plates were 4 inches (10.2 cm) long. Each series consisted of either five or six individual tests.

Figure 10 shows this data, along with the theoretically predicted line, where the span was not considered to be changed by the support. The slope of a line through this data is about the same as that for a line through the data taken with no upstream-edge support (fig. 7, p. 15). Thus, the effects of materials and geometries are about the same regardless of upstream-edge support. Upstream-edge support increased the dynamic pressure at failure by a factor of about 2.4. Scatter was considerably reduced, and all failures were sudden as indicated by visual or pressure indications. Thus, the condition of the leading edge is important, and therefore the theoretical prediction (eq. (2)), which neglects the edge condition, does not accurately predict the dynamic pressure at failure.

Modes of Plate Failure

Two basic modes of plate failure were observed during tests without upstream-edge support. The first was a sudden and complete failure of the test plate from its neutral position. The second mode of plate failure was a gradual deflection of the plate from its neutral position with increasing flow, until it touched the electrical contact or, on occasion, developed severe vibration, which produced intermittent electrical contact followed by complete failure.

For the aluminum plates tested without upstream support, about half the failures were sudden. For the copper and lead plates tested, also without upstream support, most failures (88 percent) were gradual. Although the data scatter was large for either type failure, the average dynamic pressure for gradual failures of aluminum plates was only about 5 percent lower than that for sudden failures. Since the difference is so small, both sudden and gradual failures are discussed together.

During the tests with upstream-edge point support, the failures were always sudden. In an attempt to determine the mode of sudden failure initiation, high-speed moving pictures were taken during three of these tests. Figure 11 shows a sequence of high-speed film frames taken during initiation of failure of an aluminum plate. The pins supporting the upstream edge are on the right side of each picture; the arrow shows the flow direc-

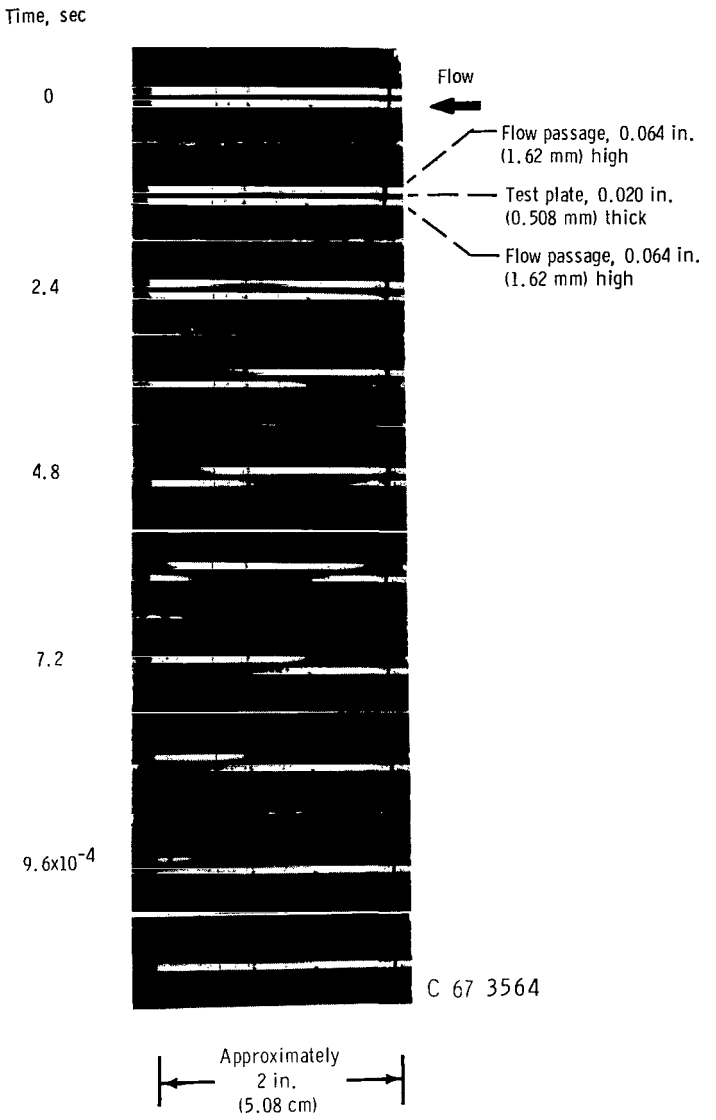

Figure 11. - High speed motion-picture frames of plate failure.

tion. Only about 2 inches (5.08 cm) of the upstream portion of the plate is shown. The film frame rate was in the range of 8000 to 9000 frames per second.

In the figure, the initial deflection appears to be downward at the upstream edge of the plate (right side of the figure) and upward near the center of the plate. Following this a wavelike motion of the plate is observed, moving downstream along the plate at a velocity of about 450 to 500 feet per second (137 to 152 m/sec) as indicated by the film frame rate. This velocity range is the same as that of the air passing over the plate. The complete sequence of film frames shows less than one cycle of plate motion before the

plate comes to rest in the flowing air. The other two similar tests, not illustrated, showed as many as five complete cycles before the motion stopped. Thus, what appeared to be a sudden failure was really something like flutter followed by permanent deformation.

SUMMARY OF RESULTS

The results of an experimental investigation to determine the dynamic pressure at failure for single flat plates are presented. These results were compared with an existing theoretical analysis which predicts critical dynamic pressure (the dynamic pressure which should cause sudden, complete plate collapse). The experimental results agree, in general, with the theoretical prediction for the effect of the material properties, but disagree with the prediction for the effect of the plate and flow-channel dimensions. A modification based on edge effect was made to the theoretical analysis which improved the accuracy of the prediction. Also, a large amount of data scatter was present in the experimental results. Some probable reasons for the lack of agreement with the theoretical prediction and for the data scatter are leading-edge effect, flutter, and turbulence, as well as other factors presently unknown.

Lewis Research Center,
National Aeronautics and Space Administration,
Cleveland, Ohio, October 26, 1967,
122-28-02-04-22.

APPENDIX - EDGE-EFFECT CALCULATIONS

by A. F. Lietzke

Since Miller considers a central portion of the plate, his equation does not account for what happens at the upstream and downstream edges. There are two effects which should be considered. The first is the increased deflection of the plate (as a beam) near the edges. The second is the angle of attack produced by the deformation of the edge of the plate when the whole plate bends as a beam.

An estimate of the edge effect is obtained by using an equation from reference 8. This equation describes the position of any point along the surface of a prismatical bar in pure bending. Thus, the position and angle of attack of the edge of the beam can be calculated and their effect on pressure determined.

Area Change Modification

This calculation was performed to obtain the ratio by which the flow-area change at the upstream edge is altered by the edge effect. To do this requires knowledge of the position of the edge relative to the average position of the plate.

Figure 12 shows a prismatical bar bent by two equal and opposite couples. This situation is considered to be analogous to the bending of a beam with built-in ends. Ref-

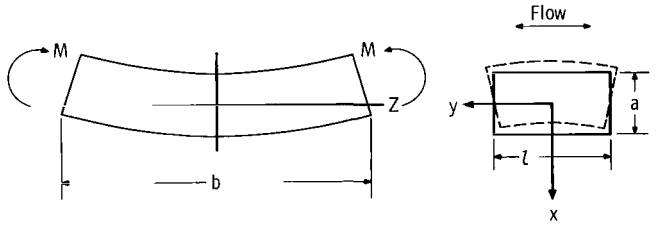

Figure 12. - Prismatical bar bent by two equal and opposite couples.

erence 8 gives an equation for the position of any point on the surface of the bar. The following three qualifications are made in using the equation:

(1) The shape of the cross section is independent of the position along the bar in the z-direction.

(2) The equation describes the centerline of the plate as shown in figure 13.

(3) The l dimension cannot exceed the b dimension, where b is the plate span

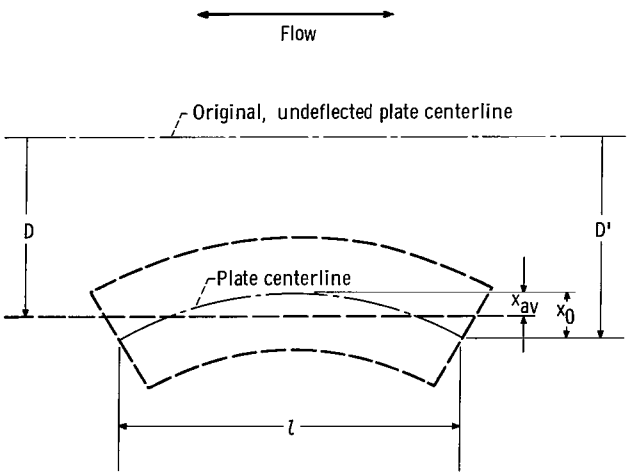

Figure 13. - Enlarged view of prismatical bar showing relative deflections.

perpendicular to l, the length in the flow direction. Reference 9 treats the buckling of flat sheets with sides restrained and concludes that when the length is greater than the span, the plate "tends to act as a series of square plates with buckles in each square, since it is prevented from buckling in a single long wave." Thus, the plate tends to assume a wavelike shape along its lengthwise centerline with nodes separated by the distance b; therefore, l can never be greater than b in the equations about to be developed.

When applied to the situation shown in figure 13, the equation of this parabolic curvature is

$$x = \frac{\nu y^2}{2R} \tag{5}$$

where x and y are the coordinates of any point on the surface using the axes shown in figure 12 and R is the radius of curvature of the bar after bending. Referring to figure 13, the position of the end x_0 will be obtained when this equation is evaluated at $y = l/2$ which yields

$$x_0 = \frac{\nu l^2}{8R}$$

The average position of the centerline x_{av} is determined by

$$x_{av} = \text{Width} = \frac{\text{Area}}{\text{Length}} = \frac{\int_0^{l/2} x\,dy}{\frac{l}{2}} = \frac{2}{l}\int_0^{l/2} \frac{\nu y^2\,dy}{2R} = \frac{\nu l^2}{24R}$$

The absolute value of the difference

$$\left|x_{av} - x_0\right| = \frac{\nu l^2}{24R} - \frac{\nu l^2}{8R} = \frac{\nu l^2}{12R}$$

The ratio of flow-channel heights caused by this deflection is

$$\frac{D'}{D} = \frac{D + \left|x_0 - x_{av}\right|}{D} = 1 + \frac{\nu l^2}{12RD}$$

where D is the average deflection of the plate centerline and D' is the position of the edge of the plate. From beam theory, R = (EI/M) and D = ($p l b^4/384EI$) where I is the moment of inertia of the plate cross section (in.^{4} (cm^4)) and M is the bending moment (in.-lb (N-cm)). In terms of the moment at midspan, where M = ($p l b^2/24$), D = ($24Mb^2/384EI$) and then

$$\frac{D'}{D} = 1 + \frac{\nu l^2 M(384EI)}{12EI(24Mb^2)} = 1 + \frac{4\nu l^2}{3b^2}$$

Therefore,

$$\frac{\Delta A'}{\Delta A} = 1 + \frac{4\nu l^2}{3b^2} \tag{6}$$

where ΔA is the area change corresponding to the average deflection D of the plate and $\Delta A'$ is the area change at the edge of the plate.

Lift Modification

To obtain the angle of attack α introduced by this edge effect, start with equation (5)

$$x = \frac{\nu y^2}{2R} \tag{5}$$

Differentiating to get the slope at the edge gives

$$\frac{dx}{dy} = \frac{\nu}{2R} 2y$$

where $y = (l/2)$ (fig. 12) so that

$$\frac{dx}{dy} = \frac{\nu l}{2R}$$

But $R = (EI/M)$ and

$$M = -\frac{Nl^2}{12} + \frac{Nl^2}{4} - \frac{Nl^2}{8} = \frac{Nl^2}{24} = \frac{pl\,b^2}{24}$$

where N is the beam load in pounds per foot (N/cm). Since the angle is small,

$$\alpha \approx \tan \alpha = \frac{dx}{dy} = \frac{\nu l}{2R} = \frac{\nu l\, pl\, b^2}{2EI(24)} = \frac{pl^2 b^2}{48EI} \tag{7}$$

From the deflection equation, $D = (pl\,b^4/384EI)$. Rearranging yields $EI = (pl\,b^4/384D)$. Substituting this expression into equation (7) results in

$$\alpha = \frac{\nu\, pl^2 b^2 (384D)}{48 pl\, b^4} = \frac{8\nu l\, D}{b^2} \tag{8}$$

But $D = (\Delta A/b)$, where $A = hb$; therefore, $b = (A/h)$ and $D = (\Delta A h/A)$. Substituting this expression into equation (8) gives

$$\alpha = \frac{8\nu l\ \Delta A h}{b^2 A} \tag{9}$$

The equation for the lift pressure on a wing for a small angle of attack is

$$p = \frac{\rho V^2}{2g} 2\pi\alpha$$

Substituting for α from equation (9) gives

$$p = \frac{\rho V^2}{g} \pi \frac{8\nu l\, h}{b^2} \frac{\Delta A}{A} \tag{10}$$

Combination of Modifications

The equation for the pressure force caused by a small deflection of the plate is (ref. 3)

$$p = \frac{2\rho V^2}{g} \frac{\Delta A}{A} \tag{11}$$

where ΔA is the flow-area change caused by the deflection, and A is the flow area before the change. This pressure is increased by the lift force as follows (see eqs. (10) and (11)):

$$p_{total} = \frac{2\rho V^2}{g} \frac{\Delta A}{A} + \frac{\rho V^2}{g} \pi \frac{8\nu l\, h}{b^2} \frac{\Delta A}{A}$$

$$= \frac{2\rho V^2}{Ag} \Delta A \left(1 + \frac{4\pi\nu l\, h}{b^2}\right)$$

Including the area-change correction from equation (6) gives

$$p = \frac{2\rho V^2}{Ag} \Delta A \left(1 + \frac{4\pi\nu l\, h}{b^2}\right)\left(1 + \frac{4\nu l^2}{3b^2}\right)$$

When this expression is put into the equation for critical dynamic pressure, there results

$$q_c = \left(\frac{15E}{1 - \nu^2}\right)\left(\frac{a^3 h}{b^4}\right)\left[\frac{1}{\left(1 + \frac{4\pi\nu l\, h}{b^2}\right)\left(1 + \frac{4\nu l^2}{3b^2}\right)}\right] \tag{12}$$

remembering that l cannot exceed b.

REFERENCES

1. Stromquist, W. K.; and Sisman, Oscar: High Flux Reactor Fuel Assemblies Vibration and Water Flow. Rep. No. ORNL-50, Oak Ridge National Lab., June 1948.

2. Doan, R. L.: The Engineering Test Reactor. A Status Report. Nucleonics, vol. 16, no. 1, Jan. 1958, pp. 102-105.

3. Miller, D. R.: Critical Flow Velocities for Collapse of Reactor Parallel-Plate Fuel Assemblies. J. Eng. Power, vol. 82, no. 2, Apr. 1960, pp. 83-95.

4. Johansson, E. B.: Hydraulic Instability of Reactor Parallel-Plate Fuel Assemblies. Rep. No. KAPL-M-EJ-9, Knolls Atomic Power Lab., July 13, 1959.

5. Kane, J. J.: The Effect of Inlet Spacing Deviations on the Flow-Induced Deflections of Flat Plates. Nucl. Sci. Eng., vol. 15, no. 3, Mar. 1963, pp. 305-308.

6. Zabriskie, W. L.: An Experimental Evaluation of the Critical Flow Velocity Formulas for Parallel Plate Assemblies. Rep. No. 58-GL-297 (AECU-3936), General Electric Co., Oct. 31, 1958.

7. Zabriskie, W. L.: An Experimental Evaluation of the Effect of Length-to-Width Ratio on the Critical Flow Velocity of Single Plate Assemblies. Rep. No. 59-GL-209 (AECU-4388), General Electric Co., Sept. 1, 1959.

8. Timoshenko, S.; and Goodier, J. N.: Theory of Elasticity. Second ed., McGraw-Hill Book Co., Inc., 1951, pp. 250-254.

9. Bruhn, Elmer F.: Analysis and Design of Airplane Structures. Rev. ed., Tri-State Offset Co., Cincinnati, 1949 (repr. Jan. 1952), p. B2.1.

NASA-Langley, 1968 —— 12 E-4095

"The aeronautical and space activities of the United States shall be conducted so as to contribute . . . to the expansion of human knowledge of phenomena in the atmosphere and space. The Administration shall provide for the widest practicable and appropriate dissemination of information concerning its activities and the results thereof."

—NATIONAL AERONAUTICS AND SPACE ACT OF 1958

NASA SCIENTIFIC AND TECHNICAL PUBLICATIONS

TECHNICAL REPORTS: Scientific and technical information considered important, complete, and a lasting contribution to existing knowledge.

TECHNICAL NOTES: Information less broad in scope but nevertheless of importance as a contribution to existing knowledge.

TECHNICAL MEMORANDUMS: Information receiving limited distribution because of preliminary data, security classification, or other reasons.

CONTRACTOR REPORTS: Scientific and technical information generated under a NASA contract or grant and considered an important contribution to existing knowledge.

TECHNICAL TRANSLATIONS: Information published in a foreign language considered to merit NASA distribution in English.

SPECIAL PUBLICATIONS: Information derived from or of value to NASA activities. Publications include conference proceedings, monographs, data compilations, handbooks, sourcebooks, and special bibliographies.

TECHNOLOGY UTILIZATION PUBLICATIONS: Information on technology used by NASA that may be of particular interest in commercial and other non-aerospace applications. Publications include Tech Briefs, Technology Utilization Reports and Notes, and Technology Surveys.

Details on the availability of these publications may be obtained from:

SCIENTIFIC AND TECHNICAL INFORMATION DIVISION

NATIONAL AERONAUTICS AND SPACE ADMINISTRATION

Washington, D.C. 20546